Molecular ordering and phase transitions in alkanol monolayers at the water–hexane interface

Aleksey M. Tikhonov[a)]
University of Chicago, Center for Advanced Radiation Sources, and Brookhaven National Laboratory, National Synchrotron Light Source, Beamline X19C, Upton, New York 11973

Sai Venkatesh Pingali
University of Illinois at Chicago, Department of Physics, Chicago, Illinois 60607

Mark L. Schlossman[b)]
University of Illinois at Chicago, Department of Physics, Chicago, Illinois 60607
and University of Illinois at Chicago, Department of Chemistry, Chicago, Illinois 60607

(Received August 18, 2003; accepted March 30, 2004)

The interface between bulk water and bulk hexane solutions of *n*-alkanols ($H(CH_2)_mOH$, where $m=20$, 22, 24, or 30) is studied with x-ray reflectivity, x-ray off-specular diffuse scattering, and interfacial tension measurements. The alkanols adsorb to the interface to form a monolayer. The highest density, lowest temperature monolayers contain alkanol molecules with progressive disordering of the chain from the $-CH_2OH$ to the $-CH_3$ group. In the terminal half of the chain that includes the $-CH_3$ group the chain density is similar to that observed in bulk liquid alkanes just above their freezing temperature. The density in the alkanol headgroup region is 10% greater than either bulk water or the ordered headgroup region found in alkanol monolayers at the water–vapor interface. We conjecture that this higher density is a result of water penetration into the headgroup region of the disordered monolayer. A ratio of 1:3 water to alkanol molecules is consistent with our data. We also place an upper limit of one hexane to five or six alkanol molecules mixed into the alkyl chain region of the monolayer. In contrast, $H(CH_2)_{30}OH$ at the water–vapor interface forms a close-packed, ordered phase of nearly rigid rods. Interfacial tension measurements as a function of temperature reveal a phase transition at the water–hexane interface with a significant change in interfacial excess entropy. This transition is between a low temperature interface that is nearly fully covered with alkanols to a higher temperature interface with a much lower density of alkanols. The transition for the shorter alkanols appears to be first order whereas the transition for the longer alkanols appears to be weakly first order or second order. The x-ray data are consistent with the presence of monolayer domains at the interface and determine the domain coverage (fraction of interface covered by alkanol domains) as a function of temperature. This temperature dependence is consistent with a theoretical model for a second order phase transition that accounts for the domain stabilization as a balance between line tension and long range dipole forces. Several aspects of our measurements indicate that the presence of domains represents the appearance of a spatially inhomogeneous phase rather than the coexistence of two homogeneous phases. [DOI: 10.1063/1.1752888]

I. INTRODUCTION

An outstanding problem in the area of interfacial phenomena is the determination of molecular ordering of surfactants at liquid–liquid interfaces. This ordering determines the ability of surfactants to bring together on the microscopic scale dissimilar materials, such as oil and water, that prefer to be phase separated on the macroscopic scale. This ability has led to many scientific and industrial applications, especially in the areas of complex fluids, and chemical and biological systems. Although it has proven convenient to study the molecular ordering of surfactants at the water–vapor interface such studies do not probe the influence of the second bulk phase (oil) on the molecular ordering.

We use x-ray scattering and interfacial tension measurements to study a set of common and simple surfactants, long-chain alkanols, at the water–hexane interface. These studies lead to an understanding of the surfactant and water ordering at the interface that includes details of the ordering in both the alkyl chain and headgroup regions of the surfactant. Comparison of these studies to a measurement at the water–vapor interface for one of the alkanols illustrates significant differences in the molecular ordering at the two interfaces. These experiments also probe the structure of the monolayer as a function of temperature, as the monolayer passes through a phase transition. X-ray reflectivity measurements over a wide range of temperature can be fit with a single parameter that characterizes the fraction of interface covered by monolayer condensed-phase domains. Equilibrium thermodynamics indicates that this interfacial structure is a spa-

[a)]Electronic mail: tikhonov@bnl.gov
[b)]Electronic mail: schloss@uic.edu

tially inhomogeneous phase. We also comment upon the order of the phase transition.

Amphiphilic surfactants often contain alkyl chains and a significant experimental and theoretical effort has been devoted to the study of long-chain surfactants containing a single alkyl chain such as fatty acids, alcohols, and esters.[1] These molecules are known to form condensed phases at the water–vapor interface. Here, we focus on long-chain normal alkanols, $H(CH_2)_mOH$ (abbreviated C_mOH in this paper). Although the primary concern of this paper is the study of long-chain alkanols at the water–hexane interface, we will review first the behavior of alkanols at the water–vapor interface for comparison.

Using ellipsometry and x-ray diffraction Berge and Renault observed the crystallization of *n*-alkanol (octanol, C_8OH, up to tetradecanol, $C_{14}OH$) monolayers at the water–vapor interface.[2] Surface x-ray diffraction from the adsorbed layer produced one Bragg peak whose width and position indicated that the alkanol molecules were hexagonally close-packed in a structure very similar to the rotator phase R_{II} of bulk alkanes.[3,4] At higher temperatures the Bragg peak disappeared as the monolayer melted. X-ray reflectivity of these alkanol monolayers (C_{10} through C_{16}) yielded the layer thickness and electron density in both the solid and liquid monolayer phases.[5]

It is known that molecules in the condensed phases of longer chain alkanol (and also alkanoic acid) Langmuir monolayers are nearly all-trans rigid rods. X-ray surface diffraction studies of Langmuir monolayers of heneicosanol ($C_{21}H_{43}OH$) demonstrated that four ordered, close-packed phases are present over the temperature range of 14 °C to 30 °C and surface pressures from 0 to 25 mN/m.[6,7] These four phases are distinguished by their lattice structures and chain tilt direction. In the highest pressure phase (surface pressure $\geqslant$20 mN/m) the molecules are upright.[6–8] The alkanols formed rigid rod phases throughout the entire range of pressures studied, down to nearly 0 mN/m.[6,7] X-ray surface diffraction studies of the normal alkanols $C_{23}H_{47}OH$, $C_{30}H_{61}OH$, and $C_{31}H_{63}OH$ at 5 °C reported similar results of ordered all-trans molecules with an average tilt of 9° from the vertical.[9,10] In a recent brief report of some of the work discussed here, we presented x-ray reflectivity studies of a Langmuir monolayer of the $C_{30}OH$ alkanol that demonstrated the presence of nearly all-trans chains and is consistent with the earlier surface diffraction work.[11] Vibrational sum frequency spectroscopy studies of Langmuir monolayers of hexacosanoic acid ($C_{26}H_{53}O_2H$) and hexadecanol ($C_{16}H_{33}OH$) indicated the absence of gauche conformations in the condensed phases,[12,13] though IR reflection spectroscopy of stearyl alcohol ($C_{18}H_{43}OH$) and heneicosanol monolayers indicated the presence of some gauche conformers whose number decreases with increasing surface pressure.[14,15]

The earliest study of the liquid–liquid interface between water and an alkane solution of alkanols (C_8OH through $C_{12}OH$) used interfacial tension measurements to demonstrate that the alkanols were adsorbed to the water–octane interface.[16] More recent interfacial tension measurements demonstrated that the adsorbed alkanol layer (for alkanols as long as $C_{18}OH$) at the water–oil interface undergoes a phase transition from a condensed to a dilute layer, in which the alkanols desorb from the interface, either as a function of temperature, bulk pressure, or alkanol concentration.[17–20]

There is a general expectation that soluble molecules at a water–oil interface are more disordered than at a water–vapor interface due to intermixing of the solvent into the monolayer.[21,22] Davies observed that the surface pressure, for a given molecular area, is usually higher at the water–oil interface than at the water–vapor interface.[21,23] Davies explained this effect by postulating that a cohesive surface pressure (of negative value and due to van der Waals attractions between the surfactant chains) that is present in films at the air–water interface is absent at the oil–water interface as a result of extensive intermixing of the solvent into the monolayer.[21,23] Pethica and co-workers discussed similar ideas in their studies of lipids at the water–oil interface.[24,25]

Until recently, direct structural information on molecular ordering in monolayers at the water–oil interface was unavailable. Here, we mention the few recent nonlinear optical and X-ray scattering measurements that have been used to compare surfactant ordering at water–oil and water–vapor interfaces.[26,27] In these studies, the systems exhibited a similar level of surfactant disorder at both of the interfaces. Nonlinear optical studies probed the ordering of short surfactants, sodium dodecylsulfonate and sodium dodecylbenzenesulfonate (DBS), to demonstrate that the alkyl chain conformations are similar at both the water–vapor and water–CCl_4 interfaces, though the benzene rings in DBS orient differently at the two interfaces.[28] Nonlinear optical studies of sodium dodecylsulfate indicated a large degree of conformational disorder at both interfaces.[29,30] X-ray reflectivity was used to study partially fluorinated dodecanol (soluble in hexane) at the water–vapor and water–hexane interfaces.[31,32] Again the chain ordering is similar at both interfaces, in this case the chain is rigid and no solvent is mixed into the monolayer. However, in two recent brief reports of some of the work discussed here, x-ray measurements revealed a large difference in the molecular conformation of $C_{30}OH$ alkanols at the water–hexane and water–vapor interfaces.[11,33] The alkanol chains at the water–vapor interface are nearly all-trans, but the chains at the water–hexane interface are disordered.

In this paper we present data for shorter alkanols at the water–hexane interface, $C_{20}OH$, $C_{22}OH$, and $C_{24}OH$, in addition to the data describing $C_{30}OH$ at the water–hexane and water–vapor interfaces. It is seen that the molecular conformation previously reported for $C_{30}OH$ is characteristic of these alkanols at the water–hexane interface. X-ray diffuse scattering measurements at low temperature confirm the structure proposed from the reflectivity measurements. We also present interfacial tension and x-ray measurements as a function of temperature for all four alkanols. The temperatures vary from values just above the bulk saturation temperature to values that pass through a phase transition, including temperatures far above the phase transition. These systems form domains at the interface and undergo a phase transition from a dense, low temperature phase to a dilute, high temperature phase.

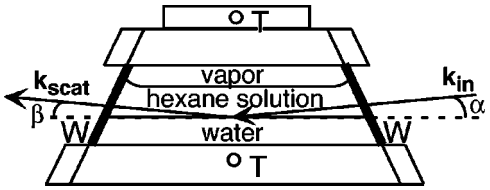

FIG. 1. Cross-sectional view of sample cell; W- mylar windows; T-thermistors to measure temperature. The kinematics of surface x-ray reflectivity is also indicated: k_{in} is the incoming x-ray wave vector, k_{scat} is the scattered wave vector, α is the angle of incidence, and β the angle of scattering ($\beta=\alpha$ for specular reflection).

II. EXPERIMENT

A. Materials

Normal hexane, purchased from Fluka (>99.5%, puriss grade), was purified in a chromatography column by passing the alkane a dozen times through a thick (~10 cm) layer of basic alumina purchased from Supelco (~100 g of alumina per 200 ml of hexane was used). The purity of the hexane was judged adequate if the water–hexane interfacial tension was constant to within ±0.1 mN/m over several hours where time is measured from the initial formation of the water–hexane interface.[34] Water was produced by a Nanopure UV Barnstead system. Purum grades of 1-eicosanol (≥97% $C_{20}OH$), 1-docosanol (≥98% $C_{22}OH$), 1-tetracosanol (≥98% $C_{24}OH$), and 1-triacontanol (~98% $C_{30}OH$) were purchased from Fluka and recrystallized twice in the purified *n*-hexane. After crystallization, the alkanol crystal flakes were collected into an air-tight glass tube and refrigerated at −18 °C until used.

The alkanol solutions in hexane were prepared in a dry glass flask placed inside an ultrasonic bath. The concentrations of the alkanols in hexane were chosen to place the phase transition in the adsorbed layers into a convenient temperature range (15 mmol/kg for $C_{20}OH$, 7 mmol/kg for $C_{22}OH$, 3 mmol/kg for $C_{24}OH$, and 0.7 mmol/kg for $C_{30}OH$). Below a temperature at which the solution becomes saturated, bulk crystals of alkanol (either flakes or whiskers) appear at the water–hexane interface. At this saturation temperature the interfacial tension is between 20 and 30 mN/m for all four systems. The experiments reported here are for temperatures above the saturation temperature.

B. Liquid–liquid sample cell

The X-ray measurements presented here are from liquid samples that are stirred and allowed to reach thermal equilibrium in a vapor-tight stainless steel sample cell that is discussed in detail elsewhere.[31,35] The sample is stirred with a teflon stir bar to ensure thermal equilibration, though the stirring was always turned off during the x-ray measurements. The interfacial area was 76 mm×100 mm (along the beam×transverse) with x-rays penetrating through the upper phase, the hexane solution (see Fig. 1). At the chosen x-ray wavelength ($\lambda=0.825\pm0.002$ Å) the absorption lengths for hexane and water are ~19 and 5.6 mm, respectively. The sample cell is contained in a two-stage cylindrical aluminum thermostat (two active stages) and temperature controlled to ±0.003 °C. The temperature variation across the x-ray footprint (varying from 0.5 to 1.5 cm long by 0.2 cm wide) was less than 0.001 °C. Thermistors mounted immediately above and below the liquid chamber measure the sample temperature and allow us to determine when the sample cell has thermally equilibrated. A pressure release valve in the gas phase above the bulk liquids is open during temperature changes so the bulk pressure is very close to atmospheric pressure.

The stainless steel sample cell was washed with soap, methanol, acetone, and pure water. Finally the sample cell was soaked for several hours first in hot (~70 °C) water, then in hot hexane to remove impurities. The sample was formed by placing ~100 ml of water into the sample cell, aspirating the water surface after waiting for 15 min, then adding ~50 ml of the hexane solution of alkanol.

C. Liquid–vapor sample cell

In addition to the measurements at the water–hexane interface, $C_{30}OH$ monolayers were also studied at the water–vapor interface. These monolayers were spread on a home built teflon Langmuir trough[36] from a 2.1 mM chloroform solution at a low density (50 $Å^2$/molecule), then compression cycled eight times between surface pressures of 0 and 25 mN/m (with addition of pure chloroform at high pressures) to create a stable, homogeneous monolayer.

D. Interfacial tension measurements

The interfacial tension of the water–hexane interface was measured in the stainless steel sample cell mounted in a thermostat consisting of just one of the two stages normally used for X-ray measurements. The Wilhelmy plate technique was used with a plate made from chromatography paper hooked to a platinum wire attached to a Cahn RH electrobalance. The plate was fully submerged in the hexane. For the tension measurements, the top plates of the sample cell and the thermostat had small holes for passage of the platinum wire (evaporation of the liquids was negligible). X-ray measurements were conducted with top plates without these holes.

E. X-ray reflectivity and diffuse scattering techniques

X-ray scattering was conducted at beamline X19C at the National Synchrotron Light Source (Brookhaven National Laboratory, USA) with a liquid surface instrument and measurement techniques described in detail elsewhere.[37,38] A similar instrument was used at the ChemMatCARS sector 15 at the Advanced Photon Source (Argonne National Laboratory) to study the monolayer of $C_{30}OH$ at the water–vapor interface.[39] The kinematics of specular reflectivity and surface diffuse scattering in the plane of incidence are illustrated in Fig. 1. Specular reflection occurs when $\beta=\alpha$ (in-plane $Q_x=Q_y=0$, normal to the interface $Q_z=(4\pi/\lambda)\sin(\alpha)$, $\lambda=0.825\pm0.002$ Å is the x-ray wavelength). Therefore, specular reflection probes structure normal to the interface, but averaged over the in-plane region of

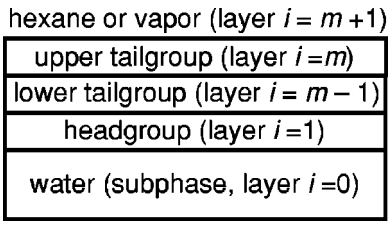

FIG. 2. Nomenclature for layers. Three layers are usually used to model the surfactant layers ($m=3$). These include two layers for the tailgroup and one for the headgroup. Some fits in Table I are for two layers ($m=2$ with only one layer for the tailgroup). Each interface has an interfacial width that characterizes the crossover of the composition of one layer (or bulk) to its neighboring layer.

the x-ray footprint on the interface. Surface diffuse scattering is measured by fixing the incident angle α and scanning the scattered angle β.

The reflectivity and diffuse scattering data consist of measurements of the x-ray intensity reflected or scattered from the sample interface normalized to the incident intensity measured just before the x-rays strike the interface. The reflectivity data are further modified by subtracting a background measured as previously described.[37,40] To set the incident beam size and vertical divergence two slits placed ~60 cm apart were used immediately prior to the liquid sample. The slit gaps were typically 5 to 10 μm in the vertical at the smallest reflection angles (horizontal slit gaps were 10 mm, much larger than the horizontal beam size of ~2 mm). The sample was followed by a pair of slits that set the vertical angular acceptance of the detector to be $\Delta\beta = 1.2\times10^{-3}$ radians for the reflectivity and $\Delta\beta = 3.5\times10^{-4}$ radians for the diffuse scattering.

Tests for radiation damage were made throughout the x-ray measurements, including repeat measurements on the same sample and on new samples. No radiation damage was evident.

F. X-ray reflectivity analysis

The surfactant monolayers are described by two or three layers sandwiched between bulk water and the bulk hexane solution (or vapor, see Fig. 2). For three layer fits layer 1 is the headgroup region ($-CH_2OH$), layers 2 and 3 are the alkyl tailgroup region [$-(CH_2)_{m-2}CH_3$]; layers are ordered water-1-2-3-hexane (or vapor). A general formula for the electron density gradient normal to a surface with m layers is[41]

$$\frac{d\langle\rho(z)\rangle}{dz}=\sum_{i=0}^{m}(\rho_i-\rho_{i+1})\frac{1}{(2\pi\sigma_{i+1}^2)^{1/2}}e^{-(z-D_i)^2/2\sigma_{i+1}^2}, \quad (1)$$

where ρ_0 is the electron density of the water, ρ_{m+1} is the density of hexane, and the Gaussian provides a smooth crossover between layers i and $i+1$ with an interfacial width σ_{i+1}. If L_i is the thickness of the ith layer, then $D_i=\Sigma_{j=1}^{i}L_j$ is the distance from the surface of the water to the interface between the ith and $(i+1)^{st}$ layers. Note that the quoted electron densities in this paper are normalized to the value for bulk water (e.g., $0.3333e^-/Å^3$ at $T=25\,°C$). As a guide to fitting the reflectivity data, the minimum number of layers is chosen that can reasonably account for the structure in the data.

Given the electron densities of each layer and the subphase, as well as the widths for each interface, the specular reflectivity is calculated from the Born approximation for x-ray scattering. This approximation relates the reflectivity to the electron density gradient normal to the interface, $d\langle\rho(z)\rangle/dz$ (averaged over the interfacial plane),[42] and written as

$$\frac{R(Q_z)}{R_F(Q_z)}\approx\left|\frac{1}{\Delta\rho_{e,\mathrm{bulk}}}\int_{-\infty}^{\infty}dz\frac{d\langle\rho_e(z)\rangle}{dz}\exp(iQ_zz)\right|^2, \quad (2)$$

where $\Delta\rho_{e,\mathrm{bulk}}$ is the electron density difference between water and bulk hexane (e.g., $\rho_{\mathrm{hexane}}=0.230e^-/Å^3$ at 20 °C), and $R_F(Q_z)$ is the Fresnel reflectivity predicted for an ideal, smooth and flat interface that has a step-function change in the electron density when going from one bulk phase to the other[43,44]

$$R_F(Q_z)\approx\left|\frac{Q_z-Q_z^t}{Q_z+Q_z^t}\right|^2, \quad \text{for } Q_z>Q_c, \quad (3)$$

where $Q_z^t=(Q_z^2-Q_c^2)^{1/2}$ and the critical wave vector for total reflection is $Q_c=4[\pi r_e(\rho_{\mathrm{water}}-\rho_{\mathrm{hexane}})]^{1/2}\approx0.012\ Å^{-1}$ ($r_e=2.818$ fm is the classical electron radius).

At the highest temperatures (above the phase transition), the surfactant monolayer has mostly desorbed from the interface and the reflectivity can be fit with an expression for a simple interface (no layers) given by[43,44]

$$R(Q_z)\approx\left|\frac{Q_z-Q_z^t}{Q_z+Q_z^t}\right|^2\exp(-Q_zQ_z^t\sigma^2). \quad (4)$$

where σ is the interfacial width.[45] This expression for the reflectivity corresponds to the following electron density profile predicted by capillary wave theory:

$$\langle\rho(z)\rangle=\frac{1}{2}(\rho_{\mathrm{water}}+\rho_{\mathrm{thexane}})+\frac{1}{2}(\rho_{\mathrm{water}}-\rho_{\mathrm{nexane}})\mathrm{erf}[z/\sigma\sqrt{2}]$$

$$\text{with } \mathrm{erf}(z)=\frac{2}{\sqrt{\pi}}\int_0^z e^{-t^2}dt. \quad (5)$$

In the original capillary wave theory, the interfacial width is due solely to interfacial roughening by capillary waves.[46] The hybrid model of the interface describes an intrinsic structural profile roughened by capillary waves. In this case, the interfacial width σ can be represented as a combination of an intrinsic profile width σ_0 and a resolution dependent capillary wave contribution,[47–50]

$$\sigma^2\equiv\sigma_0^2+\sigma_{\mathrm{cap}}^2=\sigma_0^2+\frac{k_BT}{4\pi^2\gamma}\int\int\frac{d^2\mathbf{q}}{q^2+\xi_{\parallel}^{-2}}=\sigma_0^2+\frac{k_BT}{2\pi\gamma}\ln\frac{q_{\max}}{q_{\min}}, \quad (6)$$

where k_BT is Boltzmann's constant times the temperature, γ is the interfacial tension, the correlation length, $\xi_\parallel$, is given by $\xi_\parallel^2=\gamma/\Delta\rho_m g$ and determines the exponential decay of the interfacial correlations given by the height–height correlation function of interfacial motion, $\Delta\rho_m$ is the mass density difference of the two phases, and g is the gravitational acceleration. Integration is over in-plane capillary wave vectors q corresponding to the range of capillary waves that the measurement probes. The approximation in Eq. (6) is calculated by choosing $q_{\max}$ (the cutoff for the smallest wavelength capillary waves that the interface can support), and using $q_{\min}=(2\pi/\lambda)\,\Delta\beta\sin\alpha$ determined by the incident angle α and the angular acceptance of the detector $\Delta\beta$.[49–51] The correlation length $\xi_\parallel$ can be neglected since $q_{\min}\gg\xi_\parallel^{-1}$. We have chosen $q_{\max}=2\pi/5$ Å^{-1} where 5 Å is a typical nearest neighbor distance of closest approach for alkanes, though there is little theoretical guidance for the correct choice of $q_{\max}$. The logarithm in Eq. (6) indicates that the integral is not sensitive to small changes in $q_{\max}$.

For intermediate temperatures, the interface is not a simple homogeneous surfactant monolayer, but consists of domains of a condensed phase of surfactants separated by gaseous regions of the interface (the latter is a region of very low concentration of surfactants). If the spatial coherence length of the x-rays in the plane of the interface ($\sim$5 μm) is much larger than the domains, then the x-rays reflected from neighboring domains interfere nearly coherently. If the domains are much larger than the coherence length then the interference between neighboring domains is nearly incoherent. If incoherent, then the intensity of the reflected electromagnetic fields should add; if coherent, the amplitudes of the reflected electromagnetic fields will add. An example of incoherent reflectivity is given by

$$R_{\mathrm{inc}}(T)=CR_1+(1-C)R_2, \tag{7}$$

where R_1 and R_2 are the normalized x-ray reflectivities from the condensed and gaseous domains, respectively, whose electron densities are given by Eqs. (1) and (5). The domain coverage C is the fraction of interface covered by the condensed domains.[52] Similarly, for coherent reflectivity

$$R_{\mathrm{coh}}(T)\propto|CA_1+(1-C)A_2|^2, \tag{8}$$

where A_1 and A_2 are the reflectivity amplitudes of the condensed and gaseous domains, respectively, at the interface. The reflectivity depends linearly on the domain coverage for incoherent reflectivity and quadratically for coherent reflectivity. The latter is seen explicitly by using the electron density models in Eqs. (1) and (5) to yield an expression for the coherent reflectivity

$$R_{\mathrm{coh}}(Q_z)=R_F(Q_z)(aC^2+bC+d^2)\exp(-\sigma_{\mathrm{cap}}^2Q_z^2);$$

$$a=\left[\mathrm{Re}\left(\sum_{j=0}^{m}(\rho_j-\rho_{j+1})\exp(iD_jQ_z)\right)-d\right]^2$$

$$+\mathrm{Im}^2\left(\sum_{j=0}^{m}(\rho_j-\rho_{j+1})\exp(iD_jQ_z)\right), \tag{9}$$

$$b=2d\left[\mathrm{Re}\left(\sum_{j=0}^{m}(\rho_j-\rho_{j+1})\exp(iD_jQ_z)\right)-d\right],$$

$$d=(\rho_0-\rho_m)\exp(-\sigma_0^2Q_z^2/2).$$

Equation (9) is based upon the assumption that the origin of the z axis is at the water–hexane interface in gaseous domains and at the water–headgroup ''interface'' in condensed domains, i.e., the surface of the water is at the same level throughout the sample. The solution of the quadratic equation for the domain coverage in Eqs. (8) or (9) yields two solutions. We have chosen the solution that results in a decrease in coverage with increasing temperature above the transition, as opposed to the other solution that has coverage increasing with temperature. A more complete treatment of the effects of coherence would consider the partial coherence of the x-ray beam and could be important if the domain sizes were similar to the x-ray coherence length. In this paper we limit our discussion to the approximations presented in Eqs. (7) and (8).

G. Surface diffuse scattering analysis

This technique provides information complementary to the x-ray reflectivity because the wave vector transfer contains a component in the plane of the interface as well as out of plane. The in-plane component probes structure in the plane of the interface such as capillary wave fluctuations or in-plane inhomogeneities.

The scattered intensity is determined by the Distorted Wave Born approximation,[47] given by

$$I_{\mathrm{diff}}=\frac{I_0}{\sin\alpha}\frac{Q_c^4}{256\pi^2}\int d\beta\,d\phi\,|T(\alpha)|^2|T(\beta)|^2|\Phi(\sqrt{Q_zQ_z^t})|^2$$

$$\times\frac{\exp[-\sigma^2\,\mathrm{Re}(Q_z^t)^2]}{|Q_z^t|^2}\int d^2r(e^{|Q_z^t|^2C(r)}-1)e^{iQ_{xy}\cdot\mathbf{r}}, \tag{10}$$

where I_0 is the incident intensity, α and β are the incident and scattering angles, Q_c is the critical wave vector for total internal reflection, ϕ is the in-plane scattering angle, $T(\alpha)$ and $T(\beta)$ are the Fresnel transmission coefficients, Φ is the Fourier transform of the derivative of the intrinsic electron density profile along the interfacial normal (not including capillary wave roughening of the profile), Q_z^t is the z component of the momentum transfer with respect to the water [defined after Eq. (3)], σ is the interfacial roughness, and C(r) is the height–height correlation function due to capillary waves. Complete definitions of these quantities are given by Mitrinovic *et al.*[40] For the fitting in this paper, we simplified the expression in Eq. (10) by (1) integrating analytically in ϕ from $-\infty$ to $+\infty$ to approximate our coarse resolution in that direction and (2) approximating the exponential in the integral as its two lowest order terms.[40] The latter approximation is appropriate for our data since $Q_z^2\sigma^2\ll1$ for our diffuse scattering measurements.

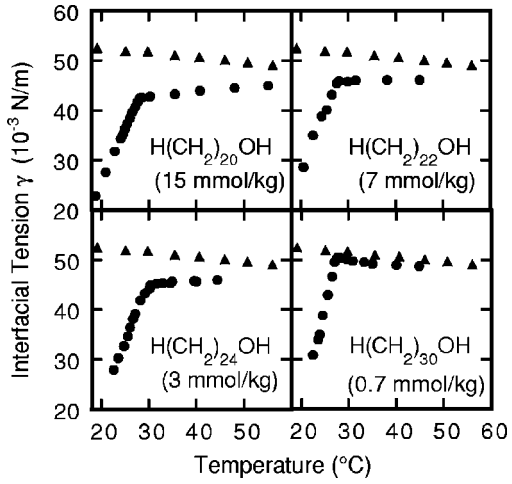

FIG. 3. Interfacial tension as a function of temperature for alkanols at the water–hexane interface (dots) and, for comparison, the pure water–hexane interface (triangles). Concentrations of the hexane solutions of alkanols are shown in the figure.

III. DATA AND ANALYSIS

A. Interfacial tension data

Figure 3 shows our measurements of interfacial tension γ as a function of temperature for four alkanols ($C_{20}OH$, $C_{22}OH$, $C_{24}OH$, and $C_{30}OH$) at the water–hexane interface and for the pure water–hexane interface.[53] The sharp change in slope reveals an interfacial transition. Above the transition the tension approaches values for the pure water–hexane interface. For $C_{30}OH$ the tension above the transition is almost the same as that for the pure interface. This indicates, at least for $C_{30}OH$, that the interface is almost completely free of surfactants above the transition. These measurements are consistent with earlier tension measurements on $C_{18}OH$ at the water–hexane interface that demonstrated a large change in interfacial density across the transition.[17]

The interfacial excess entropy per unit area is given by $S_a^\sigma = -\mathrm{d}\gamma/\mathrm{dT}$ and the change in the interfacial excess entropy across the transition ΔS_a^σ is given by the difference in S_a^σ on either side of the transition. This change ΔS_a^σ is 2.0, 2.3, 2.4, and 4.3 mJ/m^{2}K, respectively, for the $C_{20}OH$, $C_{22}OH$, $C_{24}OH$, and $C_{30}OH$ alkanols.[54] These measurements indicate that the alkanol monolayers undergo a single transition from a low temperature ordered phase to a high temperature disordered phase. These results are consistent with values measured by other groups using the pendant drop method to yield $\Delta S_a^\sigma = 1.7$ mJ/m^{2}K for $C_{18}OH$ and $\Delta S_a^\sigma = 2.0$ mJ/m^{2}K for $C_{20}OH$ at the water–hexane interface (the $C_{20}OH$ value was measured for concentrations of both 11.25 and 18.04 mol/kg).[17,55]

The values of ΔS_a^σ are much larger than the values reported previously for surface freezing at a pure alkanol–vapor interface ($\Delta S_a^\sigma = 0.88$, 1.15, 1.2, and 1.3 mJ/m^{2}K for $C_{20}OH$, $C_{22}OH$, $C_{24}OH$, and $C_{28}OH$, respectively, where these values are half that for freezing of a bilayer in order to facilitate comparison with our monolayer).[56] Our values of ΔS_a^σ are also much larger than the values of ΔS for the bulk rotator–liquid transition (measured for the bulk, but here stated for an effective "monolayer" of bulk material, $\Delta S_a = 1.09$, 1.2, and 1.35 mJ/m^{2}K for $C_{20}OH$, $C_{22}OH$, and $C_{24}OH$).[56–58] The much greater change in entropy for our transition than for a solid to liquid monolayer transition is consistent with other evidence presented in this manuscript that the alkanol monolayer transition is not surface freezing. It is reasonable to expect a larger ΔS_a^σ in our system since the transition occurs when alkanol molecules in a dilute bulk solution form a condensed monolayer at the interface [three-dimensional gas to nearly two-dimensional (2D) condensed phase], rather than the freezing of a single layer of molecules (nearly 2D liquid to nearly 2D rotator solid). An additional contribution to ΔS_a^σ may be due to ordering of water or hexane molecules that are adjacent to or within the monolayer, as discussed later.

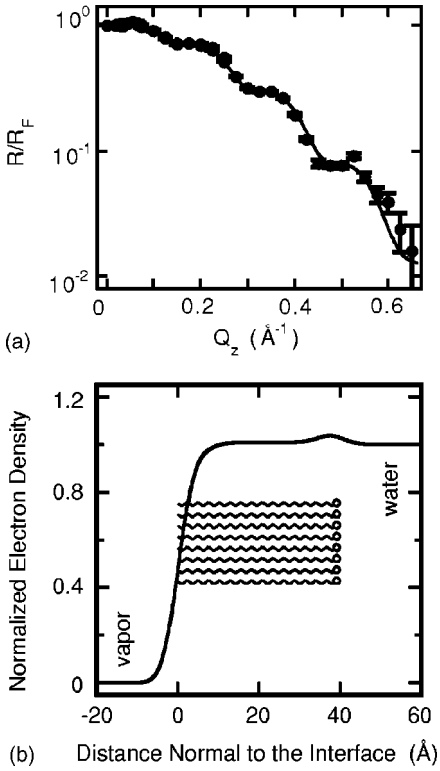

FIG. 4. $C_{30}OH$ (triacontanol) monolayer at the water–vapor interface ($T = 24\,^\circ$C, surface pressure 21.5 ± 0.5 mN/m). (a) X-ray reflectivity (normalized to the Fresnel reflectivity) as a function of the wave vector transfer normal to the interface. Line is a fit described in the text. (b) Normalized electron density profile (normalized to the value for water). The molecules order as nearly rigid rods.

B. Reflectivity from alkanol monolayers

1. $C_{30}OH$ alkanol at the water–vapor interface

We first describe the $C_{30}OH$ alkanol monolayer at the water–vapor interface to provide a reference to judge the monolayers at the water–hexane interface. Figure 4(a) shows an x-ray reflectivity measurement from a $C_{30}OH$ monolayer spread at the water–vapor interface. Oscillations in the reflectivity represent interference minima and maxima from x-rays scattered off different parts of the monolayer.

Figure 4(b) illustrates the electron density profile for the $C_{30}OH$ monolayer at the water–vapor interface determined

TABLE I. Fitting parameters for fits to the alkanol monolayer x-ray data. Layer 1 is the headgroup region (-CH_2OH), layers 2 and 3 are for the tailgroup region; layers are ordered water-1-2-3-hexane (or vapor); L is the layer thickness; L_{trans} is the calculated length of the all-trans alkanol ($L_{trans}=(n-1)\times 1.27$ Å(C–C)$+1.5$ Å(-CH_3)$+2.4$ Å(-CH_2OH)); ρ is the electron density; σ is the interfacial roughness; σ_{cap} is the roughness calculated from the measured interfacial tension using the capillary wave theory. The electron densities are normalized to the value for bulk water ($0.3333e^-/Å^3$ at $T=25\,°C$). The normalized hexane density is 0.692 at $T=20\,°C$. For the headgroup (layer 1) the maximum electron density is also quoted because the density and layer thickness fitting parameters are strongly correlated for this thin layer, but the resultant profile is well determined. The parameter N is not a fitting parameter, but is the total number of electrons per area in the monolayer determined by the fitted electron density profile.

	Layer 1			Layer 2		Layer 3						
System	L_1 (Å)	ρ_1	ρmax	L_2 (Å)	ρ_2	L_3 (Å)	ρ_3	σ (Å)	σcap (Å)	Ltotal (Å)	Ltrans (Å)	N ($e^-/Å^2$)
Low temperature:												
Water–hexane interface												
2-layer fits:												
$C_{20}OH$ (19.4 °C)	$8^{\pm 5}$	$1.15^{+1/-0.1}$	$1.07^{\pm 0.02}$	0	0	$17^{\pm 1.5}$	$0.80^{+0.01/-0.02}$	$4.7^{+0.3/-1}$	4.7	$24^{\pm 4}$	28.0	$7.6^{\pm 0.7}$
$C_{22}OH$ (21.6 °C)	$13^{+2/-7}$	$1.10^{+0.2/-0.02}$	$1.11^{\pm 0.02}$	0	0	$17^{+1/-0.3}$	$0.80^{\pm 0.01}$	$3.5^{\pm 1}$	4.2	$29^{+2/-4}$	30.6	
3-layer fits:												
$C_{22}OH$ (21.6 °C)	$4^{+6/-2}$	$1.28^{+0.4/-0.2}$	$1.12^{+0.01/-0.02}$	$9^{\pm 3}$	$0.95^{+0.15/-0.05}$	$14^{\pm 3}$	$0.79^{+0.02/-0.01}$	$3.1^{\pm 1}$	4.1	$27^{\pm 2}$	30.6	$8.2^{+0.4/-0.3}$
$C_{24}OH$ (21.9 °C)	$5^{+4/-3}$	$1.24^{+0.4/-0.1}$	$1.12^{\pm 0.005}$	$10^{+1/-1.5}$	$0.95^{+0.05/-0.03}$	$14^{\pm 1}$	$0.81^{\pm 0.01}$	$3.3^{+0.5/-1}$	4.5	$29^{+4/-1}$	33.1	$9.0^{+0.5/-0.4}$
$C_{30}OH$ (24.5 °C)	$4^{+5/-2}$	$1.32^{+0.3/-0.2}$	$1.13^{\pm 0.01}$	$13^{\pm 2}$	$0.95^{+0.02/-0.03}$	$18^{\pm 1}$	$0.79^{\pm 0.01}$	$3.4^{+0.4/-0.6}$	3.8	$35^{+4/-1}$	40.7	$10.6^{+0.5/-0.4}$
Water–vapor interface												
$C_{30}OH$ (24 °C)	$5^{\pm 4}$	$1.07^{+0.2/-0.03}$	$1.04^{\pm 0.01}$	$24^{\pm 4}$	$1.014^{\pm 0.003}$	$11^{\pm 4}$	$0.99^{+0.01/-0.04}$	$3.25^{+0.1/-0.25}$	3.24	$40^{\pm 2}$	40.7	$13.5^{+0.2/-0.1}$
High temperature (1-parameter fits):												
$C_{20}OH$ (45.45 °C)								$5.5^{\pm 0.2}$	3.7			
$C_{22}OH$ (45.65 °C)								$5.0^{\pm 0.2}$	3.6			
$C_{24}OH$ (45.25 °C)								$5.0^{\pm 0.2}$	3.5			
$C_{30}OH$ (45.02 °C)								$4.8^{\pm 0.3}$	3.8			

by fitting the reflectivity data to the model in Eq. (1) (see Table I for model parameters). Best fits for a 1-, 2-, and 3-layer model have χ^2 values of 55, 13, and 6, respectively, indicating the necessity of having a headgroup in the model and a preference for using two layers to describe the tailgroup. The overall thickness of the monolayer at the water–vapor interface is 40 ± 2 Å, nearly identical to the length of an all-trans $C_{30}OH$ molecule, calculated to be 40.7 Å.[59–61] Most of the region of the monolayer corresponding to the alkyl chain has a normalized electron density of 1.014 ± 0.003 (normalized to the value for water of $0.333\ e^-/Å^3$). This is comparable to literature values for the alkyl chain density in *bulk* phases of long chain alkanols of 1.03 or 0.985 (determined from 23.3 or 24.4 $Å^3$ per -CH_2- group for the γ_4 or β_{01} bulk phases, respectively, see Table 8-6 in Small[60]). This comparison indicates that most of the chain is close-packed. The fit shown in Fig. 4(b) requires a slightly lower electron density ($0.99+0.01/-0.04$) towards the -CH_3 group. Although this 3-sigma difference between the densities of the two layers of the tailgroup is a weak effect, it is consistent with molecular dynamics simulations that predict a small percentage of gauche conformations in these nearly rigid rod monolayers with the gauche defects concentrated near the -CH_3 end.[62,63]

The electron density profile allows us to calculate N, the number of electrons per area of the interface (see Table I) by integrating just the monolayer part of the profile over the distance normal to the interface (equivalently, $N=0.333\Sigma_{i=1,3}\rho_i L_i$). Using the area per molecule of 18.7 $Å^2$ determined by x-ray surface diffraction for a condensed monolayer of $C_{30}OH$ molecules at the water–vapor interface[10] yields 252 ($=18.7\times 13.5$) electrons per molecule. This compares well with the 250 electrons of a $C_{30}OH$ molecule.

A previous x-ray surface diffraction study of a $C_{30}OH$ monolayer at the water–vapor interface determined that the molecules are tilted from the interfacial normal by 7.7°.[10] If present, this small tilt angle would reduce the layer thickness by 1%, well within the error bars of our reflectivity measurement.

This analysis demonstrates that the $C_{30}OH$ monolayer at the water–vapor interface is close packed with nearly all-trans and nearly upright molecules (normal to the interface). This is consistent with other measurements, discussed in the Introduction, on Langmuir monolayers of alkanols. In contrast, we will show that alkanol monolayers at the water–hexane interface have a well defined disorder along the chain.

2. Alkanols at the water–hexane interface: Low temperature

a. X-ray reflectivity data. Figure 5 illustrates x-ray reflectivity measurements (normalized to the Fresnel reflectivity) from the four alkanols at the water–hexane interface at nearly the lowest temperatures shown in Fig. 3, and an example of two unnormalized reflectivity measurements for the $C_{30}OH$ monolayer. These temperatures are one to two degrees above the temperature at which the bulk hexane is saturated with the alkanols (as observed by the formation of crystallites).

The number of oscillations in the reflectivity data strongly determines our ability to interpret these data in terms of an electron density profile. Experimentally the accessible number of oscillations is limited by the monolayer

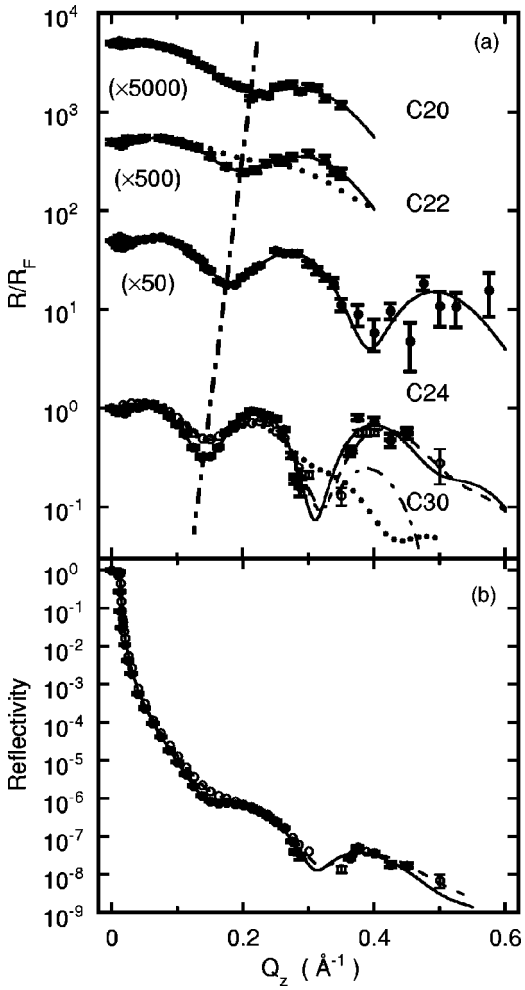

FIG. 5. Alkanol monolayers at the water–hexane interface (low temperature). (a) X-ray reflectivity (normalized to the Fresnel reflectivity) as a function of the wave vector transfer normal to the interface. At the chosen temperatures the monolayers are in a condensed phase: $C_{20}OH-19.4\,°C$; $C_{22}OH-21.6\,°C$; $C_{24}OH-21.93\,°C$; $C_{30}OH-24.1\,°C$ (filled circles and solid line fit), and 24.5 °C (open circles and dashed line fit). Curves have been offset for clarity. Lines are fits described in the text. A two layer model is used for $C_{20}OH$ and $C_{22}OH$; three layer models are used for $C_{22}OH$, $C_{24}OH$, $C_{30}OH$, though it is not possible to distinguish visually the two and three layer models for $C_{22}OH$ for this set of data. The dotted lines for the $C_{22}OH$ and $C_{30}OH$ (24.5 °C) data show a best, though inadequate, fit to the one and two layer models, respectively. A short-long dashed line for the $C_{30}OH$ (24.5 °C) data indicates a best fit two-layer model for surface freezing, it is also inadequate (it rises above the second peak of the open circles (hard to see) and drops below the third peak). Straight short-long dashed line indicates the position of the first minima (for viewing purposes only). (b) X-ray reflectivity (not normalized) for $C_{30}OH$ monolayer, legend as in panel (a).

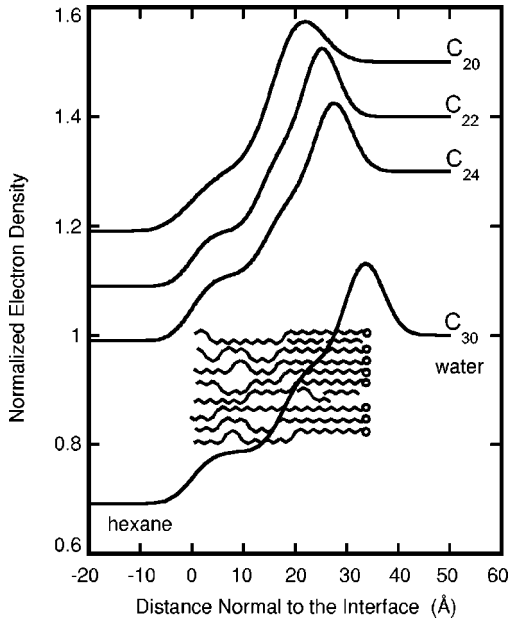

FIG. 6. Normalized electron density profiles normal to the interface for alkanol monolayers at the water–hexane interface (for low temperature data shown in Fig. 5, see Table I for profile parameters, the profile for $C_{30}OH$ at 24.5 °C is shown). The profiles for the three shorter alkanols have been offset for clarity. The alkyl chains in the monolayer at the water–hexane interface are progressively disordered from a relatively ordered region near the water to a disordered liquidlike region adjacent to bulk hexane. Hexane is mixed with the monolayer alkyl chain and water is mixed with the headgroup region. In the cartoon the long molecules represent the $C_{30}OH$ surfactants and the short molecules in the water–hexane monolayer region represent hexane. Cartoon of molecules is for illustrative purposes only.

thickness and the range in Q_z. The latter is limited primarily by the background scattering from the top phase.

The decrease in the oscillation period for longer alkanols indicates that the monolayers get thicker as chain length increases (see short-long dashed straight line in Fig. 5). The measurement of three oscillations for the two longer alkanols provides a higher spatial resolution in interpreting the x-ray reflectivity. Three layers are required to fit the data for $C_{24}OH$ and $C_{30}OH$ (two layers represent the alkyl chain and one layer represents the headgroup). An example of the best two layer fit for $C_{30}OH$ is shown by a dotted line in Fig. 5, it is clearly inadequate. Two layer models cannot fit the intensity in the third reflectivity maximum as measured for $C_{24}OH$ and $C_{30}OH$. An example of a nearly best two-layer fit that models the electron density profile expected for surface freezing (based upon parameters in Gang *et al.*[56]) is shown by the long-short dashed line that was fit to the open-circle $C_{30}OH$ data. This surface freezing fit rises above the second peak (though this is hard to see) and drops below the third peak. Constraining this fit to match the third peak results in a second peak that is more than twice as high as the data.

Since only two oscillations could be measured for the two shorter alkanols, $C_{20}OH$ and $C_{22}OH$, the data can be adequately fit with a two layer model (one layer for the tailgroup and one layer for the headgroup). A one layer model is incapable of fitting these data as illustrated by the best one layer fit for $C_{22}OH$ shown by a dotted line in Fig. 5. A three layer model for the shorter alkanols is not as well constrained by the data and yields larger error bars. For $C_{22}OH$ we have listed parameters for both the two and three layer models in Table I. For $C_{20}OH$ the two and three layer models yield essentially the same electron density profile. Since the three layer model for $C_{20}OH$ has such large error bars, we have just listed the parameters for the two layer model.

b. Electron density profiles. Figure 6 shows electron density profiles normal to the water–hexane interface for the alkanol monolayer data in Fig. 5. Comparison with Fig. 4(b) shows a large difference between profiles at the water–vapor and water–hexane interfaces. Although the parameters are most accurately determined for the $C_{30}OH$ and $C_{24}OH$

monolayers, Table I shows that the electron density parameters are very similar for the alkanol monolayers at the water–hexane interface. The normalized electron densities for the two layers representing the chain are ~0.95 and 0.80, both different from the value of 1.03 (or 0.985) for the alkyl chain density in the γ (or β) close-packed *bulk* phases of long chain alkanols.[60] However, the density of 0.95 is comparable to the density in the α or rotator phases of long chain alkanes.[60] The volume per -CH_2- in the alkane rotator phases varies from 25 to 26 Å^3 which corresponds to a normalized density of 0.96–0.92 (see Figs. 2–6 and 7–11, and Table 7–5 in the reference by Small).[60] The alkyl chain region of surface frozen alkanols in the rotator phase has a similar density of 0.93.[56]

The volume per -CH_2- for the alkyl chains of bulk liquid alkanes and alkanols just above their freezing point is 29.6 Å^3 which corresponds to a normalized density of 0.81 (see Fig. 2–4 and Table 8–6 in Small[60]). This is very similar to the average value of 0.80 measured for layer 3 (see Table I) and indicates the presence of gauche conformations over more than half of the chain.[64,65]

The disorder in the chain will account, at least partially, for the overall monolayer thickness for each of the monolayers being slightly less than the length of the corresponding all-trans alkanol molecule, see Table I. A single kink defect (gtg' or g'tg conformation) will maintain the overall chain orientation while reducing its length by 0.6–0.7 Å. It is not clear how many of these defects should be expected in the chain. Bulk liquid alkanes are expected to have a gauche fraction of about 0.45 from x-ray diffraction, but 0.35 from IR spectroscopy.[64,65] IR spectroscopy of lipid bilayers in the fluid phase indicates an overall gauche fraction of 0.14 in the alkyl chain.[65] These numbers lead to an expectation of approximately five gauche conformations per alkanol chain, leading to a reduction in the chain length of ~2 Å if only kink defects are present. This accounts for most of the difference between the measured monolayer thickness and the all-trans length. However, other defects, such as gg, may be present that decrease the monolayer thickness by a greater amount.

Additional decrease of the monolayer thickness may be due to a tilt of the molecule from the normal, however, the reflectivity does not directly probe this tilt. It is clear from the density profiles in Fig. 6 that the monolayer at the water–hexane interface does not consist of all-trans, tilted molecules that are often found at the water–vapor interface. In that case, the density profile would have a similar shape as the profile at the water-vapor interface shown in Fig. 4, but would be thinner by a factor of $\cos\theta$, where θ is the tilt from the normal. In addition, the density profile can not be explained by a model of the chain that has a uniform amount of disorder along the chain (with or without tilting). This two-layer profile would also have a similar shape as the profile in Fig. 4. As discussed, two-layer profiles are unable to fit the $C_{24}OH$ and $C_{30}OH$ data (see Fig. 5). Instead, the measured profiles indicate a progressive disordering of the chain from the headgroup to the terminal methyl group.

Since the headgroup region (-CH_2OH) is small, the thickness parameter L_1 of the headgroup layer is strongly correlated with the electron density ρ_1 of the headgroup layer. This correlation is responsible for the large error bars in this region (see Table I). However, inspection of the electron density profiles for different fits (not shown) within the range of the error bars shows that the profiles are nearly indistinguishable. To parameterize this region, we list the maximum electron density ρ_{max} in the headgroup region (i.e., the maximum value for each profile in Fig. 6) in Table I. As indicated by the small error bars on ρ_{max}, this parameter is nearly unchanged for different choices of L_1 and ρ_1 within the range of errors quoted in Table I. The value of ρ_{max} in the headgroup region is larger at the water–hexane interface for all the alkanols (typically, $\rho_{max}=1.12\pm0.01$) than at the water–vapor interface for $C_{30}OH$ ($\rho_{max}=1.04\pm0.01$, with $\rho_{bulk\ water}=1$). As will be discussed, the area per headgroup is larger at the water–hexane interface due to disorder in the monolayer, therefore, the additional electron density cannot be attributed to closer packing of headgroups. In addition, the higher density is not likely due to the interaction of water with hexane since x-ray measurements of the pure water–hexane interface do not reveal an enhanced interfacial density of water.[35] We suggest that the larger area per headgroup at the water–hexane interface allows for water penetration into the headgroup region which then results in a higher density in this region.

c. Area per molecule and molecular makeup of the monolayer. One approach to determining the area per molecule is to assume that the agreement between the average value of 0.80 for the electron density in layer 3 (the terminal part of the tailgroup) of all these alkanol monolayers and the electron density of liquid alkyl chains for bulk alkanols just above their freezing point, 0.81, indicates that this layer has a similar molecular order as liquid alkyl chains. A disordered liquid alkyl chain with a normalized electron density of 0.81 occupies a surface area of ~23.4 Å^2/chain and, by our assumption, indicates that the area per alkanol molecule for these monolayers is ~23.4 Å^2.[60] A simple check that an area per molecule of 23.4 Å^2 is reasonable is to divide the number of electrons per alkanol molecule by the measured number of electrons per area (N in Table I). This yields $22.4^{\pm2}$, $22.7^{\pm1}$, $22.4^{\pm1}$, and $23.6^{\pm1}$ Å^2 for $C_{20}OH$, $C_{22}OH$, $C_{24}OH$, and $C_{30}OH$. All of these values are within error bars of 23.4 Å^2.

One consequence of an area per alkanol molecule of 23.4 Å^2 is additional space in the headgroup region since the area occupied by the headgroup is 18.7 Å^2 (as determined from the close packed phase at the water–vapor interface).[10] Assuming that the area and volume ratios scale similarly, 20% [=(23.4−18.7)/23.4] of the volume in the headgroup region can be occupied by water. The values of 40.6 Å^3 for the -CH_2OH volume (determined by bulk measurements just above the freezing point[60]) and 30 Å^3 for the volume per bulk water molecule indicate that there is enough space for one water molecule for every 3 alkanol headgroups in layer 1. Including these additional 3 electrons per alkanol from the water that penetrates the headgroup region would raise the values of area per molecule calculated in the previous paragraph to $22.8^{\pm2}$, $23.0^{\pm1}$, $22.8^{\pm1}$, and $23.9^{\pm1}$ Å^2 for $C_{20}OH$, $C_{22}OH$, $C_{24}OH$, and $C_{30}OH$. These values are still consistent with an area per alkanol molecule of 23.4 Å^2.

As discussed, the electron density in layer 2, 0.95, is comparable to the density in rotator phases of long chain alkanes.[60] Surface freezing measurements at the surface of an alkanol melt indicate that the area per molecule in the surface rotator phase is 20.3 $Å^2$.[56] If the chain ordering in layer 2 is the same as for the rotator phase, then there is an unoccupied area per alkanol in this layer of 3.1 $Å^2$ (=23.4–20.3). Given the thickness of layer 2 (see Table I), the unoccupied volume per alkanol in this layer varies from 30 to 40 $Å^3$ depending upon chain length. If hexane intercalates into the monolayer to fill this volume, then there would be one hexane for every five or six alkanol molecules (a hexane molecule in a rotator phase occupies a volume of ~190 $Å^3$, see Fig. 8-3 in Small).[60] Alternatively, it is possible that the alkanol chain in layer two has a different conformation that fills up layer 2. Therefore, our estimate on the number of intercalated hexane molecules represents an upper limit. At the limit, 8–10 hexane electrons per alkanol are added to the monolayer. These additional electrons are consistent with the limits on the area per molecule previously discussed.

d. Summary. The low temperature structure of the alkanol monolayers at the water–hexane interface consists of an average area per alkanol of $23^{\pm 1}$ $Å^2$, a tailgroup region with progressive disorder from the headgroup to the terminal methyl group, tailgroup ordering near the headgroup similar to the structure in the α (rotator) bulk phases of alkyl chains, ordering in the rest of the tailgroup (more than half of the alkyl chain) similar to the conformation of liquid alkyl chains just above the freezing point of bulk alkanols, an upper limit of 1 hexane to 5 or 6 alkanols mixed into the chain region, and a headgroup region that contains a small fraction of water (~1 water to three alkanols).

3. Far above the transition temperature

At a temperature corresponding to the kinks in the tension versus temperature curves (Fig. 3) a large fraction of the adsorbed alkanol molecules leave the interface and are solvated in the bulk hexane. Measurements of the x-ray reflectivity at ~18 °C higher than this phase transition are shown in Fig. 7. All of these reflectivity measurements are without oscillations and can be fit by the model for a simple interface in Eqs. (4) and (5). In this model, the interfacial width is the only fitting parameter. Values for the width are typically 5.0 Å at high temperature, whereas the calculated contribution from capillary waves is about 3.6 Å for the four alkanol systems [see Table I and Eq. (6)]. This difference can be attributed to an intrinsic interfacial width $\sigma_0 \approx 3.5$ Å in Eq. (6). Measurements of the pure water–hexane interface determine a much smaller intrinsic interfacial width $\sigma_0 < 1.5$ Å,[35] indicating that the large width at high temperatures in the alkanol systems should be attributed to the presence of a small number of alkanol molecules at the interface.

4. Intermediate temperatures near the transition

As the temperature is increased from the lowest temperatures for the data in Fig. 5 the amplitude of oscillations in the reflectivity progressively decreases until the oscillations have disappeared entirely as shown for the highest temperatures in Fig. 7. Abbreviated reflectivity curves, consisting of six or seven values of Q_z (typically from 0.075 to 0.225 $Å^{-1}$ in steps of 0.025 $Å^{-1}$), were measured for many different temperatures for $C_{22}OH$, $C_{24}OH$, and $C_{30}OH$. For $C_{20}OH$, full reflectivity curves were measured at all temperatures (to be published elsewhere). The variation of reflectivity with temperature can be viewed by plotting the reflectivity at a fixed Q_z as a function of temperature, as illustrated in Fig. 8. The shape of the temperature dependent reflectivity at fixed Q_z varies with the specific choice of Q_z, but all the measurements shown in Fig. 8 have a sharp feature that occurs at the phase transition indicated by the kink in the interfacial tension curves in Fig. 3 (the sharp feature is also present for each system at the other Q_z values that were measured, but not shown in Fig. 8). The lines in Fig. 8 are fits to a theory discussed later in Sec. IV B.

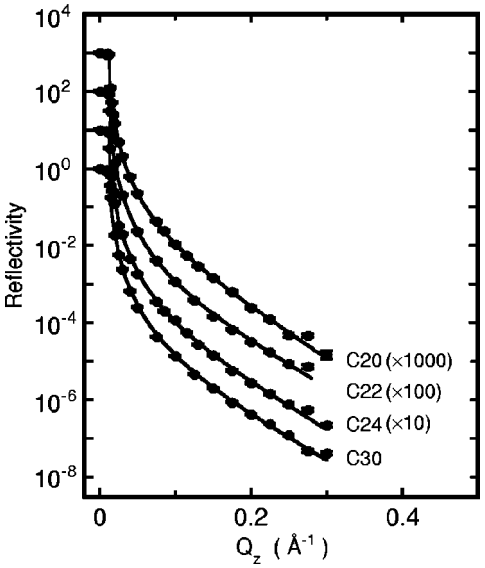

FIG. 7. Reflectivity for alkanol monolayers at the water–hexane interface far above the transition temperature (see Table I under the heading "High temperature" for the temperatures and fit parameters). The fits are for a simple interface without a monolayer of surfactants.

Figure 9 illustrates values for domain coverage determined from the data in Fig. 8. The reflectivity data at all intermediate temperatures (excluding the lowest and highest temperature for each alkanol) are fit using Eqs. (7) and (8) that describe the monolayer in terms of domains. R_1 and R_2 (or A_1 and A_2) are chosen to be the x-ray reflectivities (or amplitudes) determined from the fits to the lowest temperature data and the highest temperature data, respectively. The domain coverage (the fraction of the interface covered by domains of the condensed phase) is the only fitting parameter used to fit the intermediate temperature data. However, for each intermediate temperature the interfacial roughness is fixed to the value calculated by capillary wave theory using Eq. (6). This calculation used our measured values of the interfacial tension for that temperature and an intrinsic profile width $\sigma_0 = 0$ for the condensed phase and $\sigma_0 = 3.5$ Å for the gas phase (as determined by our lowest and highest temperature measurements). Our ability to fit all the data at intermediate temperatures with one fitting parameter provides strong support for the presence of domains at the interface.

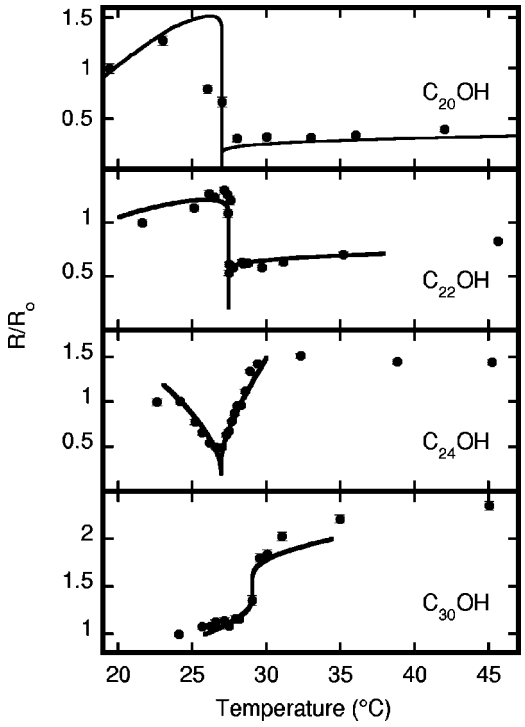

FIG. 8. Reflectivity as a function of temperature at a fixed Q_z (0.275 Å^{-1} for $C_{20}OH$, 0.2 Å^{-1} for $C_{22}OH$, 0.175 Å^{-1} for $C_{24}OH$, 0.15 Å^{-1} for $C_{30}OH$). The reflectivity is normalized by R_0, the value of reflectivity at the lowest temperature shown. The fits, represented by lines, are determined by the Marchenko model discussed in the Discussion section (this model is valid only near the phase transition). For $C_{20}OH$, $C_{22}OH$, and $C_{24}OH$, the fits use coherent reflectivity, but for $C_{30}OH$ incoherent reflectivity is used.

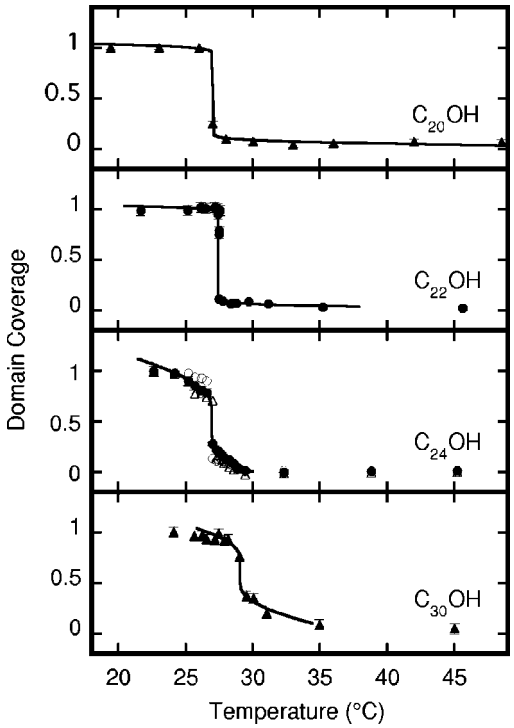

FIG. 9. Domain coverage as a function of temperature determined from the data in Fig. 8. Domain coverage is the fraction of the interface occupied by condensed phase domains. Dots illustrate domain coverage determined by coherent reflectivity, filled triangles are determined from incoherent reflectivity (though the data in Fig. 8 for $C_{20}OH$ cannot distinguish between the two types of reflectivity). The fits, represented by lines, are determined by the Marchenko model discussed in the Discussion section (this model is valid only near the phase transition). For $C_{24}OH$ two additional data sets, not shown in Fig. 8, are shown for $Q_z = 0.15$ Å^{-1} (open circles) and for $Q_z = 0.2$ Å^{-1} (open triangles) as an example of the consistency of the coverage curves for data measured at different values of Q_z.

The curves in Fig. 9 all show a nearly fully covered interface at the lowest temperatures, followed (for $C_{24}OH$ and $C_{30}OH$) by a gradual decrease in domain coverage until the transition temperature is reached. At the transition, the domain coverage changes abruptly, and is then followed by a gradual decrease in domain coverage to nearly zero at the highest temperatures. The coverage for $C_{20}OH$ and $C_{22}OH$ changes from a value of nearly one to nearly zero at the transition. A self-consistent check on the one-parameter fitting is that domain coverage curves calculated from reflectivity at different values of Q_z are all similar. An example of this is shown for $C_{24}OH$ in Fig. 9 that illustrates the coverage determined from reflectivity measured at three different values of Q_z (0.15, 0.175, and 0.2 Å^{-1}). The overall shapes of the curves in Fig. 9 are similar to domain coverage curves previously published for $F(CF_2)_8(CH_2)_2OH$ and $F(CF_2)_{10}(CH_2)_2OH$ monolayers at the water–hexane interface.[32] The fits illustrated in Fig. 9 will be discussed later.

Analysis of a reflectivity curve at a single temperature may be consistent with either or both coherent and incoherent reflectivity [see Eqs. (7) and (8)]. However, the temperature dependence provides us with more information to make the choice between coherent and incoherent reflectivity. We base this discussion on the plausible expectation that the coverage varies monotonically with temperature. Equation (7) predicts that incoherent reflectivity is only applicable if the reflectivity at fixed Q_z changes monotonically with temperature. Therefore, the reflectivity data for $C_{24}OH$ in Fig. 8 are not consistent with incoherent reflectivity, though they are well fit by coherent reflectivity. In this case, Eqs. (8) and (9) demonstrate that the dip in the temperature dependence of the data for $C_{24}OH$ can be explained with coherent reflectivity. Note also that the $C_{24}OH$ data cannot be explained by a homogeneous monolayer that changes its density monotonically with temperature. The dip in these data require the existence of regions of the interface that produce different reflected x-ray fields that interfere coherently. Similarly, the temperature dependence for $C_{22}OH$ is only consistent with coherent reflectivity and that for $C_{30}OH$ data is only consistent with incoherent reflectivity. Analysis of Eq. (9) using the parameters for $C_{20}OH$ indicates that a very small dip of 5%–7% would be predicted for coherent reflectivity as a function of temperature (compare to the large dip in the $C_{24}OH$ data), but the accuracy of these data is insufficient to determine a dip this shallow. The full reflectivity curves very close to the transition for $C_{20}OH$ cannot be fit properly with coherent reflectivity, however, the overall temperature dependence shown in Fig. 8 is more consistent with coherent reflectivity. Fortunately, the coverage curves for $C_{20}OH$ are essentially independent of the choice of coherent or incoherent reflectivity.

Identifying the reflectivity as either coherent or incoher-

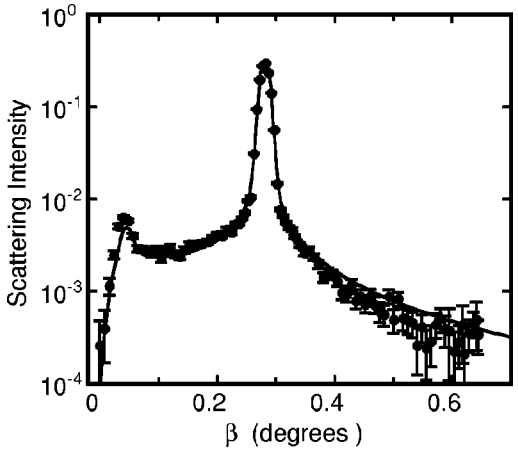

FIG. 10. X-ray off-specular diffuse scattering from $C_{24}OH$ at 21.9 °C. The only meaningful fitting parameter to produce the line is a small constant background (9×10^{-5}). The large peak at $\beta=0.28$ degrees is the specular reflection, the small peak of diffuse scattering occurs at the critical angle for total reflection. The agreement between line and data confirms the model used for the x-ray reflectivity.

ent provides some guide as to the domain size, though it is not definitive. For example, condensed phase domains smaller than the x-ray coherence length in the interface (~5 μm) that are separated by much larger regions of gas phase would be fit by coherent reflectivity. Similarly, condensed phase domains much larger than the coherence length separated by large regions of gas would be better fit by incoherent reflectivity. However, it is possible that very large condensed phases that nearly fill the interface and are separated by thin regions (whose width is less than the coherence length) of gas would also be fit better by coherent reflectivity.

5. Off-specular diffuse scattering

Figure 10 illustrates x-ray off-specular diffuse scattering as a function of scattering angle β for fixed $\alpha=0.28°$ (see Fig. 1) for $C_{24}OH$ at 21.9 °C. A similar data set (not shown) was also measured for $C_{30}OH$ for temperatures below the phase transition. The line in Fig. 10 is calculated from Eq. (10) with the approximations discussed in the paragraph after that equation. Additional information needed to calculate the line include the resolution of the x-ray instrument which was determined by a slit before the detector with a 0.24 mm gap in the vertical and 10 mm gap in the horizontal (the slit is 680 mm from the sample leading to a resolution of 3.5×10^{-4}) and by two slits of 0.04 mm$\times$10 mm (separated by $\sim$0.5 m) before the sample (a resolution of 8×10^{-5}). The function Φ in Eq. (10) that contains the information about the electron density profile normal to the surface was determined by the parameters in Table I that resulted from the fitting to the x-ray reflectivity data for this system. The roughness σ was also taken to be the value determined from the reflectivity given in Table I. A very small constant background (9×10^{-5}) was fit to the diffuse scattering data.

Except for the small constant background, the diffuse scattering shown by the line in Fig. 10 was calculated from the electron density profile previously determined by the reflectivity analysis and by the measured interfacial tension of 28 mN/m at this temperature. The good agreement between the line and data in Fig. 10 confirms our analysis of the reflectivity at low temperatures.

IV. DISCUSSION

A. Alkanol conformation and water ordering

The data and analysis discussed in Sec. III demonstrates that *n*-alkanols at the water–hexane interface have disordered chains whereas our data on $C_{30}OH$ at the water–vapor interface and earlier measurements on long-chain alkanols at the water–vapor interface demonstrate that they adopt the conformation of nearly rigid rods.[6–8,11–13] The chain density in the terminal half of the chain is the same as for bulk liquid alkanes just above their freezing point. In the bulk these chains have many gauche defects.[60,64,65] Closer to the headgroups the electron density is larger, indicating that the chains are more ordered. This effect seems less pronounced as the alkanol gets shorter. Figure 6 illustrates that the larger density region of the chain near the headgroup is not required to explain our results for the shortest alkanol, $C_{20}OH$. This may be an artifact of our inability to measure to higher Q_z for the shortest alkanols or may indicate a greater disorder in the chains of $C_{20}OH$.

Our conclusion regarding a progressive distribution of gauche conformations along the alkyl chain that increases away from the $-CH_2OH$ group is sensible considering the constraints of placing a head group at the water–hexane interface and orienting the alkyl chain towards the hexane. A similar effect was observed in molecular-dynamics simulations of lipid bilayers[65] and also, though to a lesser extent, in MD simulations of Langmuir monolayers in which there are a small number of gauche conformations that appear primarily at the chain ends.[1,62] Also, in the liquid phase of bulk alkanols far from the freezing point, NMR experiments have shown that a 7 carbon long region of the alkyl chain near the $-CH_2OH$ group of 1-dodecanol $[CH_3(CH_2)_{11}OH]$ has a constant degree of order with increasing chain disorder further out along the chain.[60] In the bulk liquid, hydrogen bonding between nearest neighbor $-CH_2OH$ groups provides the constraint that establishes the pattern of chain ordering. This is a weaker constraint than that provided by the flat water–hexane interface in our experiments.

The larger area per alkanol molecule required for these disordered chains ($\sim$23 Å^2) as compared to close-packed alkanols ($\sim$19–20 Å^2) allows for water penetration into the region of the headgroups. This may be responsible for our surprising finding that the electron density in the headgroup region is larger than for headgroups in close-packed alkanol monolayers. The fact that this density is also larger than the bulk density for water indicates a special ordering of the water and headgroups for these molecules at the water–hexane interface.

We suggest that a mechanism to produce the higher density is orientational ordering of the penetrated water by the polar $-CH_2OH$. We emphasize that this mechanism is a speculation and requires further experiments and theory for its justification. However, it is sensible to expect interfacial

electric fields to align nearby water. For example, orientational ordering of interfacial water at a charged interface has been inferred or observed in several experiments. These include the observation of enhanced water density near a charged silver electrode surface[66] as well as enhanced hydrogen bonding near charged surfactants at the water–CCl_4 interface,[67,68] near the headgroups of a hexacosanoic acid monolayer at high pH at the water–vapor interface,[12] and near uncharged stearyl alcohol monolayers at the water–vapor interface.[69] Our suggested mechanism is different from this previous work. We propose that the additional space between the headgroups of the disordered alkanol monolayers allow water molecules to penetrate into the headgroup region. Alignment of the water by the interfacial field, due primarily to the polar headgroups, could lead to a higher electron density in this region. This mechanism is closely related to that recently proposed to explain observations that water in the first hydration shell of lysozyme and other proteins has an average density ~10%–20% greater than the bulk density.[70] In this case, molecular dynamics simulations attribute the higher density to orientational ordering of water molecules in depressions on the protein surface.[71,72] The density enhancement in these protein experiments is similar to our findings, however, in our system the enhanced density is in a region consisting of headgroups and water, not just in a layer of water.

B. Phase transitions

Two issues of concern are the nature of the phases on either side of the phase transition indicated by the kink in the interfacial tension curves in Fig. 3 and the order of the phase transition. First, we will compare our findings with those of surface freezing.

1. Comparison to surface freezing

The interfacial tension curves in Fig. 3 are qualitatively similar to surface tension curves measured for freezing of a layer at the liquid–vapor interface of a one-component alkane or alkanol melt for an appropriate range of chain lengths.[56,73] We summarize the surface freezing results here. Surface freezing occurs within a few degrees above the bulk freezing temperature. X-ray grazing incidence diffraction and reflectivity measurements have shown that the surface frozen layer of alkanes is a monolayer in a crystalline, rotator phase with hexagonal packing. For alkanols, the surface frozen layer is a bilayer in one of two rotator phases distinguished by the molecular tilt that can be either normal to the interface or tilted towards the next-nearest neighbors. The packing for most alkanols is hexagonal, though some show a slightly distorted hexagonal lattice. The area per molecule in the surface frozen phases is either 19.7 $Å^2$ for the alkanes or 20.3 $Å^2$ for the alkanols. These surface frozen phases consist of nearly all-trans molecular chains. The surface freezing transition occurs discontinuously in temperature within an accuracy of a few m °C. No structural changes in the frozen layer were observed over the range from the bulk freezing to the surface freezing temperature. No evidence of layering was observed above the surface freezing temperature. The surface is a homogeneous layer, i.e., without domains, in both the frozen and liquid states.

Comparison to our measurements indicates that the transition in alkanol monolayers at the water–hexane interface is not a freezing transition for a number of reasons: (1) The low-temperature condensed phase monolayer is not crystalline. As discussed, the electron density profile at low temperature is not consistent with a crystalline phase or with all-trans molecules (normal to the interface or tilted). The low-temperature phase has alkyl tails that are disordered with a liquid density for a large portion of the chain. The area per molecule is 23 $Å^2$. The liquid-like nature of the low temperature phase is consistent with BAM images of $C_{18}OH$ at the water-hexane interface that demonstrated that the shape of domains of the condensed low-temperature phase "is strongly influenced by convective flow within the interface." [74] Also, the BAM images found no evidence for regions of uniform molecular tilt as would be expected for crystalline monolayers with molecules tilted from the interfacial normal.[74] (2) The entropy change across the transition is much larger than measured for surface freezing of an alkanol monolayer or for freezing of a hypothetical monolayer in a bulk alkanol melt. (3) For $C_{30}OH$, visual inspection of the tension curve in Fig. 3 shows that above the transition, the tension is nearly identical with the tension for the pure water–hexane interface. This indicates that most of the $C_{30}OH$ molecules desorb from the interface when heated above the transition. (4) The reflectivity curves far above the transition are similar for all four alkanols and are not consistent with a monolayer of molecules that has undergone a transition from solid to liquid. The electron density contrast between bulk liquid alkanols of these chain lengths and hexane is greater than 15%. Therefore, a liquid monolayer, if present, would be easily detected by x-ray reflectivity. (5) Unlike surface freezing, the structure of the monolayer is not constant below the transition for $C_{24}OH$ and $C_{30}OH$. In addition, evidence for a partial monolayer is observed for a range of temperatures above the transition for these alkanols. (6) The temperature dependence of the reflectivity provides strong evidence for domain formation. For example, the data for $C_{24}OH$ cannot be explained by a homogeneous monolayer that changes its average density with temperature.

2. Domain phases

Earlier Brewster angle microscopy studies of $F(CF_2)_{10}(CH_2)_2OH$ and $C_{18}OH$ monolayers at the water–hexane interface and x-ray off-specular diffuse scattering studies of $F(CF_2)_{10}(CH_2)_2OH$ monolayers at the water–hexane interface directly demonstrated the formation of domains of these surfactants at the interface.[74,75] X-ray reflectivity measurements are also consistent with the formation of domains in monolayers of both $F(CF_2)_{10}(CH_2)_2OH$ and $F(CF_2)_8(CH_2)_2OH$ at the water–hexane interface.[32] Our measurements provide evidence for domain formation in normal alkanol monolayers.

The Gibbs phase rule indicates that these interfaces with domains are not coexistence regions of two interfacial phases, but rather that the interface is in a single phase that is

spatially inhomogeneous. This is a consequence of our observations that the domains are observed over a range of temperatures, that the domains are in equilibrium, and that the role of impurities seems to be negligible. To consider this in more detail we state the phase rule for our system. The thermodynamic variance w is

$$w = 2 + (c - r) - \phi - (\psi - s), \tag{11}$$

where $c = 3$ is the number of components (water, hexane, and alkanol), $r = 0$ is the number of chemical reactions, $\phi = 2$ is the number of bulk phases, $s = 1$ is the number of types of interfaces, and ψ is the number of interface phases.[76] Equation (11) is appropriate for systems in which the interface phases are contiguous (so we only consider the liquid–liquid interface) and the interface is flat.

For one interface phase, $\psi = 1$, the system is trivariant, $w = 3$, and its state is determined by specifying three intensive thermodynamic variables, such as the temperature, bulk pressure (one atmosphere in our experiments), and the concentration of the alkanol. For two interface phases, the system is divariant, $w = 2$, and two interface phases should exist only at one temperature for a chosen bulk pressure and alkanol concentration. If the domains are a coexistence between two phases, then that coexistence should occur only at one temperature. Alternatively, domains can be the result of competing interactions that yield a single, spatially inhomogeneous, interface phase.[77,78] In this case, the interfacial concentration of alkanols is not isotropic, but varies within the interface due to the presence of domains. Since this spatially inhomogeneous phase is a single interfacial phase, it can exist over a range of temperatures for a given bulk pressure and concentration.

It is also possible for domains of coexisting phases to exist over a range of temperatures due to the presence of impurities or nonequilibrium effects that invalidate the phase rule. Both of these possibilities will now be discussed.

Our earlier measurements of the sizes of domains in $F(CF_2)_{10}(CH_2)_2OH$ monolayers at the water–hexane interface demonstrated that domains can be created or annihilated as a function of temperature.[75] This can happen only if alkanol molecules can freely exchange between the bulk and the interface, indicating that there is good reason to believe these systems are in, or very close, to equilibrium.

In our earlier measurements on $F(CF_2)_{10}(CH_2)_2OH$ monolayers at the water–hexane interface we tested the role of impurities. Our initial experiments did not include purification of either the hexane or the surfactant. Eventual purification of first the hexane, then the surfactant did not lead to significant changes in the variation of the domain coverage with temperature if the sample was always heated (or cooled) through the transition. However, the least pure systems exhibited a large hysteresis ($\sim 10\,^{\circ}C$) in the transition temperature upon heating or cooling through the transition. After purification of the hexane the hysteresis was reduced to $\sim 2\,^{\circ}C$,[31] and after purification of the surfactant the hysteresis was reduced to below the level of the experimental temperature step ($0.3\,^{\circ}C$).[32] Similar measurements on purified systems of normal alkanols led to a reproducibility of the heating and cooling curves to within the size of the temperature step for that particular measurement ($0.02\,^{\circ}C$ for $C_{22}OH$ and $0.2\,^{\circ}C$ for $C_{24}OH$). These results indicate that domains are present over a wide range of impurity levels, including the low levels required to remove the hysteresis in the transition temperature.

Although these conclusions on domain equilibrium and impurities were determined from measurements on fluorinated alkanols at the water–hexane interface, it is plausible that they are also applicable to the normal alkanols. For both types of alkanols, the alkanols we studied are soluble in hexane, have similar tension curves, and similar domain coverage curves as determined by temperature dependent x-ray reflectivity measurements. These conclusions indicate that the interfaces we have measured that contain domains over a wide range of temperature are in a spatially inhomogeneous phase.

It is difficult for our measurements to distinguish between a high density domain phase with coverage near to one and a homogeneous monolayer. Similarly it is also difficult to distinguish between a phase with coverage close to zero and a homogeneous monolayer. For $C_{20}OH$ and $C_{22}OH$, Fig. 9 indicates that these monolayers may be homogeneous above and below the transition. For $C_{24}OH$ and $C_{30}OH$, Fig. 9 shows coverage values different from zero or one over a range of temperatures. In this case, the phase transition is from a low temperature, high density domain phase to a high temperature, low density domain phase.

3. Phase transition order

Our data cannot conclusively assign the order of the phase transition. As discussed below, our data provide evidence that $C_{20}OH$ and $C_{22}OH$ undergo a first order transition while $C_{24}OH$ and $C_{30}OH$ undergo either a weakly first order transition or a second order transition.

The kink in the interfacial tension curves as a function of temperature, shown in Fig. 3, indicates that the transition is first order. The sharp change in coverage illustrated in Fig. 9 for $C_{20}OH$ and $C_{22}OH$ is consistent with a first order phase transition. The gradual variation in coverage over a range of temperatures above and below the transition for $C_{24}OH$ and $C_{30}OH$ may be consistent with a weakly first-order transition, but as discussed below, it may also be a second-order transition. Several other experimental observations argue against a first-order phase transition. For purified systems (as in this paper), there is no evidence of hysteresis across the transition as expected for a first-order transition. Measurements of domain sizes in $F(CF_2)_{10}(CH_2)_2OH$ monolayers at the water–hexane interface yielded a relatively narrow distribution with a nearly temperature independent mean radius.[75] First order transitions between spatially homogeneous phases typically have a broad distribution of radii of coexisting phases, with a mean radius that varies with temperature. These observations indicate that alkanol monolayers at the water–hexane interface may undergo a transition that is higher than first order.

The theoretical literature discusses spatially inhomogeneous phases that arise from competing interactions in many areas of condensed matter physics. These include strongly correlated electron systems,[79–81] ferromagnetic films,[82–87]

TABLE II. Domain coverage parameters from Marchenko theory. Parameters for fitting the data in Figs. 8 and 9 to Eq. (12). The analysis is based upon coherent reflectivity except for $C_{30}OH$ which exhibited incoherent reflectivity.

System	T_c (°C)	a	b	$C(T_c)$
$C_{20}OH$	27.0±0.2	0.20±0.09	0.63±0.08	0.54±0.02
$C_{22}OH$	27.4±0.1	0.17±0.02	0.55±0.25	0.5±0.1
$C_{24}OH$	26.8±0.2	1.3±0.1	3.8±0.3	0.52±0.05
$C_{30}OH$	29±0.5	1.5±0.5	4 (+6/−2)	0.6±0.05
$FC_{10}OH$	27.4±0.2	1.6±0.1	2.1±0.2	0.77±0.02
$FC_{12}OH$	40.4±0.2	0.9±0.1	1.9±0.2	0.5±0.02

ferrofluids,[88] and Langmuir monolayers at the water–vapor interface.[89,90] Although the latter may seem closely related to our system, phase transitions in Langmuir monolayers may be very different than our system because the alkanols can freely exchange between the interface and the bulk whereas the surfactants in Langmuir monolayers are essentially confined to the interface. We are not aware of a theory of these phenomena that properly accounts for the role of the bulk phase as a surfactant reservoir.

These theories disagree about the order of the transition. Analytical studies have argued for a first order transition,[78,83,84,91,92] though recent numerical studies provide evidence for a continuous second order transition.[93,94] These numerical studies are consistent with an early argument by Marchenko that two-dimensional first-order phase transitions are forbidden at the surface of a liquid.[95] Based upon a theory for a dipolar Ising ferromagnet, Marchenko also suggested that a second-order transition between domain phases should occur at the surface of a liquid.[77] The domains are stabilized by a balance of their line tension and dipole interactions. Using a scaling theory and the form of these interactions, Marchenko predicted a characteristic dependence of the surface polarization with temperature.

Although the applicability of the Marchenko theory to our system needs to be further investigated, we have chosen to test it by fitting our domain coverage data. Marchenko's prediction for the polarization can be rewritten in terms of domain coverage,

$$C(T)-C(T_c)=b\ \mathrm{sign}(T_c-T)[\ln(T_c/|T_c-T|)]^{-a} \quad \text{for } T\rightarrow T_c, \tag{12}$$

where T_c is the phase transition temperature, $C(T_c)$ is the domain coverage at the transition, and a and b are positive constants related to scaling parameters in the theory. The temperature dependence of our reflectivity measurements and the resultant domain coverage are consistent with the unusual temperature dependence proposed by this theory, as illustrated by the lines in Figs. 8 and 9. Although this is a theory for a second order phase transition it is consistent with the observed sharp change in domain coverage at the transition temperature. Values for these fitted parameters are listed in Table II as well as values from two previously studied fluorinated alkanols.[32] A deficiency of Marchenko's scaling theory is that it does not provide a value for the exponent a. Experimentally, the exponent varies between 1 and 3/2 for four of the alkanols we have studied [$C_{24}OH$ and $C_{30}OH$ plus the earlier studies of $F(CF_2)_8(CH_2)_2OH$ and $F(CF_2)_{10}(CH_2)_2OH$]. However, both $C_{20}OH$ and $C_{22}OH$ have a more abrupt transition and the exponent is much smaller. As previously discussed, the variation in coverage for $C_{20}OH$ and $C_{22}OH$ is consistent with a first-order transition, therefore, Marchenko's theory may not be applicable for these two alkanols.

V. CONCLUSIONS

We have used x-ray reflectivity, off-specular diffuse scattering, and interfacial tension measurements to probe the molecular ordering and phase transitions at the interface between water and a hexane solution of alkanols (either $C_{20}OH$, $C_{22}OH$, $C_{24}OH$, or $C_{30}OH$). Our data demonstrate that the adsorbed interfacial film is a monolayer. The highest density films that are accessible in the studied temperature range (19–45 °C) contain alkanol molecules with progressive disordering of the chain from the $-CH_2OH$ to liquid ordering in the terminal half of the chain near the $-CH_3$ group. An upper limit of one hexane molecule penetrated into the chain region of every 5 or 6 alkanol molecules is consistent with our data. In contrast, $C_{30}OH$ at 24 °C at the water–vapor interface forms an ordered phase of nearly rigid rods that excludes the solvent.

At the water–hexane interface the density in the alkanol headgroup region is 10% greater than either bulk water or the ordered headgroup region found at the water–vapor interface. We conjecture that this higher density is a result of water penetration into the headgroup region of the disordered monolayer. Our data are consistent with a water to alkanol ratio of 1:3.

The alkanol monolayer at the water–hexane interface undergoes a phase transition as a function of temperature from a dense monolayer at low temperatures to a dilute monolayer at high temperatures. Our interfacial tension data indicate a significant change in interfacial excess entropy at this transition that increases with increasing chain length of the alkanol. The data for $C_{20}OH$ and $C_{22}OH$ indicate the phase transition is first order, however, the transition for $C_{24}OH$ and $C_{30}OH$ may be weakly first order or second order. The x-ray data are consistent with the presence of domains in the monolayer and determine the domain coverage (fraction of interface covered by alkanol domains) as a function of temperature. This temperature dependence is consistent with a theoretical model for a second-order phase transition that accounts for the domain stabilization as a balance between line tension and long range dipole forces. Several aspects of our measurements indicate that the presence of domains represents the appearance of a spatially inhomogeneous phase rather than the coexistence of two homogeneous phases.

ACKNOWLEDGMENTS

We acknowledge conversations with Vladimir Marchenko (Kapitsa Institute, Russia), Dirk Morr (UIC), Binhua Lin (U of Chicago), and Mark Maroncelli (Pennsylvania State University); Sarka Malkova for assisting with interfa-

cial tension measurements; Ming Li for assistance with measurements at NSLS; and the valuable assistance of Binhua Lin (U of Chicago), Guangming Luo (UIC), Mati Meron (U of Chicago), Tim Graber (U of Chicago), David Schultz (UIC), and Jeff Gebhardt (U of Chicago) in taking the water–vapor measurements at the Advanced Photon Source. M.L.S. acknowledges support from the Petroleum Research Fund administered by the ACS, the UIC Campus Research Board, and the NSF Division of Materials Research. ChemMatCARS is supported by NSF Chemistry and DOE. Brookhaven and Argonne National Laboratories are supported by the U.S. Department of Energy.

[1] V. M. Kaganer, H. Mohwald, and P. Dutta, Rev. Mod. Phys. **71**, 779 (1999).
[2] B. Berge and A. Renault, Europhys. Lett. **21**, 773 (1993).
[3] A. Renault, J. F. Legrand, M. Goldmann, and B. Berge, J. Phys. II **3**, 761 (1993).
[4] J. F. Legrand, A. Renault, O. Konovalov, E. Chevigny, J. Als-Nielsen, G. Grübel, and B. Berge, Thin Solid Films **248**, 95 (1994).
[5] J. P. Rieu, J. F. Legrand, A. Renault, B. Berge, B. M. Ocko, X. Z. Wu, and M. Deutsch, J. Phys. II **5**, 607 (1995).
[6] B. Lin, Ph.D. Thesis, Northwestern University, 1990.
[7] M. C. Shih, T. M. Bohanon, J. M. Mikrut, P. Zschack, and P. Dutta, J. Chem. Phys. **97**, 4485 (1992).
[8] S. W. Barton, B. N. Thomas, E. B. Flom, S. A. Rice, B. Lin, J. B. Peng, J. B. Ketterson, and P. Dutta, J. Chem. Phys. **89**, 2257 (1988).
[9] D. Jacquemain, F. Leveiller, S. Weinbach, M. Lahav, L. Leiserowitz, K. Kjaer, and J. Als-Nielsen, J. Am. Chem. Soc. **113**, 7684 (1991).
[10] J.-L. Wang, F. Leveiller, D. Jacquemain, K. Kjaer, J. Als-Nielsen, M. Lahav, and L. Leiserowitz, J. Am. Chem. Soc. **116**, 1192 (1994).
[11] A. M. Tikhonov and M. L. Schlossman, J. Phys. Chem. B **107**, 3344 (2003).
[12] P. B. Miranda, Q. Du, and Y. R. Shen, Chem. Phys. Lett. **286**, 1 (1998).
[13] K. Wolfrum and A. Laubereau, Chem. Phys. Lett. **228**, 83 (1994).
[14] J. T. Buontempo and S. A. Rice, J. Chem. Phys. **99**, 7030 (1993).
[15] J. T. Buontempo and S. A. Rice, J. Chem. Phys. **98**, 5835 (1993).
[16] J. J. Jasper and B. L. Houseman, J. Phys. Chem. **67**, 1548 (1963).
[17] N. Matubayasi, K. Motomura, M. Aratono, and R. Matuura, Bull. Chem. Soc. Jpn. **51**, 2800 (1978).
[18] K. Motomura, N. Matubayasi, M. Aratono, and R. Matuura, J. Coll. Int. Sci. **64**, 356 (1978).
[19] M. Lin, J.-L. Firpo, P. Mansoura, and J. F. Baret, J. Chem. Phys. **71**, 2202 (1979).
[20] T. Ikenaga, N. Matubayasi, M. Aratono, K. Motomura, and R. Matuura, Chem. Soc. Jpn. Bull. **53**, 653 (1980).
[21] J. T. Davies and E. K. Rideal, *Interfacial Phenomena*, 2nd ed. (Academic, New York, London, 1963).
[22] M. Rouhi, Chem. Eng. News **August**, 6 (1995).
[23] J. T. Davies, Proc. R. Soc. London, Ser. A **208**, 224 (1951).
[24] B. Y. Yue, C. M. Jackson, J. A. G. Taylor, J. Mingins, and B. A. Pethica, J. Chem. Soc., Faraday Trans. 1 **72**, 2685 (1976).
[25] J. A. G. Taylor, J. Mingins, and B. A. Pethica, J. Chem. Soc., Faraday Trans. 1 **72**, 2694 (1976).
[26] M. L. Schlossman, Curr. Opin. Colloid Interface Sci. **7**, 235 (2002).
[27] G. L. Richmond, Annu. Rev. Phys. Chem. **52**, 357 (2001).
[28] M. Watry and G. L. Richmond, J. Am. Chem. Soc. **122**, 875 (2000).
[29] G. R. Bell, C. D. Bain, and R. N. Ward, J. Chem. Soc., Faraday Trans. **92**, 515 (1996).
[30] J. C. Conboy, M. C. Messmer, and G. L. Richmond, J. Phys. Chem. **100**, 7617 (1996).
[31] Z. Zhang, D. M. Mitrinovic, S. M. Williams, Z. Huang, and M. L. Schlossman, J. Chem. Phys. **110**, 7421 (1999).
[32] A. M. Tikhonov, M. Li, D. M. Mitrinovic, and M. L. Schlossman, J. Phys. Chem. B **105**, 8065 (2001).
[33] M. L. Schlossman and A. M. Tikhonov, in *Mesoscale Phenomena in Fluid Systems*, edited by F. Case and P. Alexandridis (Oxford University Press, New York, 2003), pp. 81–95.
[34] A. Goebel and K. Lunkenheimer, Langmuir **13**, 369 (1997).
[35] D. M. Mitrinovic, Z. Zhang, S. M. Williams, Z. Huang, and M. L. Schlossman, J. Phys. Chem. B **103**, 1779 (1999).
[36] A. A. Acero, M. Li, B. Lin, S. A. Rice, M. Goldman, I. B. Azouz, A. Goudot, and F. Rondelez, J. Chem. Phys. **99**, 7214 (1993).
[37] M. L. Schlossman, D. Synal, Y. Guan, *et al.*, Rev. Sci. Instrum. **68**, 4372 (1997).
[38] D. K. Schwartz, M. L. Schlossman, and P. S. Pershan, J. Chem. Phys. **96**, 2356 (1992).
[39] B. Lin, M. Meron, J. Gebhardt, T. Graber, M. L. Schlossman, and P. J. Viccaro, Physica B **336**, 75 (2003).
[40] D. M. Mitrinovic, S. M. Williams, and M. L. Schlossman, Phys. Rev. E **63**, 021601 (2001).
[41] I. M. Tidswell, B. M. Ocko, P. S. Pershan, S. R. Wasserman, G. M. Whitesides, and J. D. Axe, Phys. Rev. B **41**, 1111 (1990).
[42] P. S. Pershan, Faraday Discuss. Chem. Soc. **89**, 231 (1990).
[43] M. Born and E. Wolf, *Principles of Optics*, 6 ed. (Pergamon Press, Oxford, England, 1980).
[44] L. Nevot and P. Croce, Rev. Phys. Appl. **15**, 761 (1980).
[45] According to J. Daillant, O. Belorgey, J. Chem. Phys. **97**, 5824 (1992), the effect of finite resolution should appear in Eq. (4) in the form of a gamma function. This factor takes into account the spatial resolution of the x-ray instrument and the short-wave cutoff in the spectrum of the capillary waves. Using $q_{max}=2\pi/5\ \text{Å}^{-1}$ for this cutoff and the parameters of the instrument [see M. L. Schlossman *et al.*, Rev. Sci. Instrum. **68**, 4372 (1997)] we evaluated this resolution dependence for the reflectivity. The correction for the resolution dependence is always much smaller than the error bars shown.
[46] F. P. Buff, R. A. Lovett, and F. H. Stillinger, Phys. Rev. Lett. **15**, 621 (1965).
[47] S. K. Sinha, E. B. Sirota, S. Garoff, and H. B. Stanley, Phys. Rev. B **38**, 2297 (1988).
[48] J. D. Weeks, J. Chem. Phys. **67**, 3106 (1977).
[49] A. Braslau, M. Deutsch, P. S. Pershan, A. H. Weiss, J. Als-Nielsen, and J. Bohr, Phys. Rev. Lett. **54**, 114 (1985).
[50] A. Braslau, P. S. Pershan, G. Swislow, B. M. Ocko, and J. Als-Nielsen, Phys. Rev. A **38**, 2457 (1988).
[51] D. M. Mitrinovic, A. M. Tikhonov, M. Li, Z. Huang, and M. L. Schlossman, Phys. Rev. Lett. **85**, 582 (2000).
[52] Note that our domain coverage, C, is different from the standard thermodynamic coverage (typically referred to as θ). The coverage θ refers to the total number of surfactant molecules at the interface normalized by the number of surfactant molecules in a fully covered, close-packed monolayer. Since x-ray reflectivity cannot determine the number of surfactant molecules in the very low density gas phase that often covers part of the interface, the two coverages θ and C will be slightly different.
[53] A. M. Tikhonov, M. Li, and M. L. Schlossman (BNL National Synchrotron Light Source Activity Report 2001, 2002), pp. 2.73–2.76.
[54] The measurement of ΔS^S across the transition for $C_{20}OH$ has been independently verified using the pendant drop technique by Takanori Takiue (Kyushu University, personal communication).
[55] Takanori Takiue (Kyushu University, personal communication).
[56] O. Gang, X. Z. Wu, B. M. Ocko, E. B. Sirota, and M. Deutsch, Phys. Rev. E **58**, 6086 (1998).
[57] E. B. Sirota and X. Z. Wu, J. Chem. Phys. **105**, 7763 (1996).
[58] Note that the values of ΔS for the bulk rotator–liquid transition quoted by O. Gang *et al.* (previously cited) were stated for an effective ''bilayer'' of bulk material to facilitate comparison with their frozen surface bilayer.
[59] $40.7\ \text{Å} = 29\times 1.27\ \text{Å}\ (\text{C–C}) + 1.5\ \text{Å}\ (\text{-CH3}) + 2.4\ \text{Å}\ (\text{-CH2OH})$.
[60] D. M. Small, *The Physical Chemistry of Lipids* (Plenum, New York, 1986).
[61] J. N. Israelachvili, *Intermolecular and Surface Forces* (Academic, London, England, 1992).
[62] J. Harris and S. A. Rice, J. Chem. Phys. **89**, 5898 (1988).
[63] J. P. Bareman, G. Cardini, and M. L. Klein, Phys. Rev. Lett. **60**, 2152 (1988).
[64] A. Habenschuss and A. H. Narten, J. Chem. Phys. **92**, 5692 (1990).
[65] R. G. Snyder, K. Tu, M. L. Klein, R. Mendelssohn, H. L. Strauss, and W. Sun, J. Phys. Chem. B **106**, 6273 (2002).
[66] M. F. Toney, J. N. Howard, J. Richer, G. L. Borges, J. G. Gordon, O. R. Melroy, D. G. Wiesler, D. Yee, and L. B. Sorenson, Nature (London) **368**, 444 (1994).
[67] D. E. Gragson, B. M. McCarty, and G. L. Richmond, J. Phys. Chem. **100**, 14272 (1996).
[68] G. L. Richmond, Chem. Rev. (Washington, D.C.) **12**, 2693 (2002).

[69] Q. Du, R. Superfine, E. Freysz, and Y. R. Shen, Phys. Rev. Lett. **70**, 2313 (1993).
[70] D. I. Svergun, S. Richard, M. H. J. Koch, Z. Sayers, S. Kuprin, and G. Zaccai, Proc. Natl. Acad. Sci. U.S.A. **95**, 2267 (1998).
[71] F. Merzel and J. C. Smith, Proc. Natl. Acad. Sci. U.S.A. **99**, 5378 (2002).
[72] J. C. Smith, F. Merzel, C. S. Verma, and S. Fischer, J. Mol. Liq. **191**, 27 (2002).
[73] B. M. Ocko, X. Z. Wu, E. B. Sirota, S. K. Sinha, O. Gang, and M. Deutsch, Phys. Rev. E **55**, 3164 (1997).
[74] S. Uredat and G. H. Findenegg, Langmuir **15**, 1108 (1999).
[75] M. Li, A. Tikhonov, and M. L. Schlossman, Europhys. Lett. **58**, 80 (2002).
[76] R. Defay, I. Prigogine, A. Bellemans, and D. H. Everett, *Surface Tension and Adsorption* (Longmans, Green & Co. Ltd., London, 1966).
[77] V. I. Marchenko, JETP **63**, 1315 (1986).
[78] D. Andelman, F. Brochard, and J.-F. Joanny, J. Chem. Phys. **86**, 3673 (1987).
[79] C. H. Chen and S.-W. Cheong, Phys. Rev. Lett. **76**, 4042 (1996).
[80] M. P. Lilly, K. B. Cooper, J. P. Eisenstein, L. N. Pfeiffer, and K. W. West, Phys. Rev. Lett. **82**, 394 (1999).
[81] V. J. Emery, E. Fradkin, S. A. Kivelson, and T. C. Lubensky, Phys. Rev. Lett. **85**, 2160 (2000).
[82] C. Kittel, Phys. Rev. **70**, 965 (1946).
[83] S. A. Brazovskii, Sov. Phys. JETP **41**, 85 (1975).
[84] T. Garel and S. Doniach, Phys. Rev. B **26**, 325 (1982).
[85] R. Allenspach and A. Bischof, Phys. Rev. Lett. **69**, 3385 (1992).
[86] M. Seul and R. Wolfe, Phys. Rev. A **46**, 7519 (1992).
[87] D. K. Morr, P. J. Jensen, and K. H. Bennemann, Surf. Sci. **307–309**, 1109 (1994).
[88] D. Lacoste and T. C. Lubensky, Phys. Rev. E **64**, 041506 (2001).
[89] H. M. McConnell, Annu. Rev. Phys. Chem. **42**, 171 (1991).
[90] H. Mohwald, Annu. Rev. Phys. Chem. **41**, 441 (1990).
[91] M. Seul and D. Andelman, Science **267**, 476 (1995).
[92] V. M. Kaganer and E. B. Loginov, Phys. Rev. E **51**, 2237 (1995).
[93] I. Booth, A. B. MacIsaac, J. P. Whitehead, and K. De'Bell, Phys. Rev. Lett. **75**, 950 (1995).
[94] J. Arlett, J. P. Whitehead, A. B. MacIsaac, and K. De'Bell, Phys. Rev. B **54**, 3394 (1996).
[95] V. I. Marchenko, JETP **54**, 605 (1981).